Solid state forms of 4-aminoquinaldine - From void structures with and without solvent inclusion to close packing

Doris E. Braun, Thomas Gelbrich, Volker Kahlenberg and Ulrich J. Griesser

Electronic Supplementary Information

Contents of Supplementary Information

1 Experimental Screening and Characterisation of 4-AQ Anhydrates and Solvates 2
1.1 Solid Form Screen 2
1.1.1. Evaporative Crystallisation 2
1.1.2. Cooling Crystallisation 4
1.1.3. Antisolvent Addition Crystallisation 5
1.1.4. Liquid Assisted Grinding (LAG) Experiments 6
1.2 Characterisation of 4-AQ Anhydrates and Carbon Tetrachloride Solvate 7
1.2.1. Anhydrate I° 7
1.2.2. Anhydrate II 7
1.2.3. Anhydrate III 12
1.2.3. Carbon Tetrachloride Solvate 13
1.3 Thermodynamic Stability - Semi-schematic Energy/Temperature Diagram 14
2 Computational Search for Anhydrate Polymorphs 15
2.1 Conformational Analysis of 4-Amino-2-methylquinoline 15
2.2 Computational Generation of the Crystal Energy Landscape 16
2.2.1. Space groups 16
2.2.2. DFT-D Calculations: Methodology 16
2.2.3. Lowest Energy Structures (CrystalOptimizer and PBE-D) 17
2.3 Representation of the Experimental Structures 20
2.4 PIXEL Calculations 22
2.5 Hirshfeld Surfaces 23
2.6 Computationally Generated AH III Structure 24

1 Experimental Screening and Characterisation of 4-AQ Anhydrates and Solvates

1.1 Solid Form Screen

The solid form screen encompassed a solvent crystallisation screen, thermal screening and desolvation studies. Solvent evaporation, cooling crystallisation, anti-solvent addition and liquid assisted grinding experiments were employed for the solvent screen.

1.1.1. Evaporative Crystallisation

The evaporative crystallisation screen was designed from 28 pure solvents. **4-AQ** (5–10 mg compound) was dissolved in 0.5–20 mL solvent at room temperature, then filtered either into a watch glass or vial. Vials were left open or closed with perforated caps and stored at room temperature or for faster evaporation in a drying oven at 40 °C. Residues were analysed with IR or XRPD.

The results of the evaporative crystallisation screen are summarised in Table S1. The monohydrate (**MH**) / mixture of **MH** and **AH I°** (anhydrate) was observed in the vast majority evaporation experiments at room temperature and **AH I°** at 40 °C. Additional forms, i.e. carbon tetrachloride solvate, **AH II** containing residual solvent and **AH III** were found. From dimethyl formamide and dimethyl sulfoxide a different compound crystallised at 40 °C. The latter was not further characterised.

Table S1. Summary of evaporative **4-AQ** crystallisation experiments (WG – watch glass, oV – open vial, pV – perforated vial).

Solvent	WG (RT)[a]	oV (RT)[a]	pV (RT)[a]	WG (40 °C)[a]	oV (40 °C)[a]	pV (40 °C)[a]
Methanol	□	–	–	–	–	–
Ethanol	□ > ○	–	–	–	–	–
1-Propanol	□ > ○	□	□	○	○	○
2-Propanol	□ > ○	□	□	○	○	○
1-Butanol	□+○	□	□	○	○+◇	○+◇
2-Butanol	□	□	□	○	○	○
1-Pentanol	□+○	□	□	○	○	○
2-Pentanol	□	□	□	○	○	○
t-Pentanol	□+○	□	□	○	○	○
Acetone	□	–	–	–	–	–
Acetonitrile	□+○	–	–	–	–	–
Dimethyl formamide	□+○	–	–	diff. cpd	–	–
Dimethyl sulfoxide	□	–	–	diff. cpd	–	–
Dichloromethane	□+○	□+○	□+○	○	○	○
Dichloroethane	□+○	□+○	□+○	○	○	○
Chloroform	○+◇	□+○	□+○	○	○	○
Carbon tetrachloride	X(S_{CCl4})	S_{CCl4}	S_{CCl4}	○+ X(S_{CCl4})	◇ S_{CCl4} [b]	◇ S_{CCl4} [b]
1,4-Dioxane	□+○	–	–	–	–	–
Methyl acetate	□+○	–	–	–	–	–
Ethyl acetate	□+○	–	–	–	–	–
Diethyl ether	□+○	–	–	–	–	–
Ethyl methyl ketone	○	–	–	–	–	–
Nitromethane	○+am	–	–	–	–	–
Pyridine	□	–	–	–	–	–
Tetrahydrofurane	□+○	□+○	□	○+◇	○+◇	○+◇
Toluene	□+○					
Xylene	○					
Water	□					

[a]□= MH , ○ = AH I°, ◇= AH II containing residual solvent, **X** = AH III, am = amorphous, S_{CCl4} = carbon tetrachloride solvate, diff. cpd – different compound. [b]Solution saturated at 75 °C.

1.1.2. Cooling Crystallisation

The cooling crystallisation screen was designed from 26 pure and seven mixed solvents. Suspensions of **4-AQ** (10–25 mg in 0.5–20 mL solvents) were heated to the boiling point of the solvent, then filtered into vials. The vials were closed and cooled to room temperature (vial wrapped in Al foil) or 8 °C (refrigerator). The solid product was analysed with IR or XRPD (Table S2). **MH**, **AH I°**, and the carbon tetrachloride solvate ($\mathbf{S_{CCl4}}$) were obtained.

Table S2. Summary of **4-AQ** cooling crystallisation experiments.

Solvent	RT (slow)[a]	8 °C (fast)[a]	Solvent(s)	RT (slow)[a]	8 °C (fast)[a]
Methanol	○	□	Water + methanol (1:1)	□	□
Ethanol	□	□	Water + ethanol (1:1)	□	□
1-Propanol	□	□	Water + 1-propanol (1:1)	□	□
2-Propanol	□	□	Water + 2-propanol (1:1)	□	□
1-Butanol	□	□	–	–	–
2-Butanol	□	□	–	–	–
1-Pentanol	□	□	–	–	–
2-Pentanol	□	□	–	–	–
t-Pentanol	□	□	–	–	–
Acetone	□	□	Water + acetone (1:1)	□	□
Acetonitrile	○	□+○	Water + acetonitrile (1:1)	□	□
Dichloromethane	○	□	–	–	–
Dichloroethane	○	□+○	–	–	–
Chloroform	○	□+○	–	–	–
Carbon tetrachloride	S_{CCl4}	S_{CCl4}	–	–	–
Dioxane	□+○	□+○	Water + dioxane (1:1)	□	□
Methyl acetate	□	□	–	–	–
Ethyl acetate	○	□	–	–	–
Diethyl ether	○	□	–	–	–
Ethyl methyl ketone	□+○	□+○	–	–	–
Nitromethane	○	○	–	–	–
Pyridine	□	□	–	–	–
Tetrahydrofurane	○	□+○	–	–	–
Toluene	○	□	–	–	–
Xylene	○	□	–	–	–
Water	□	□	–	–	–

[a]□= MH , ○ = AH I°, S_{CCl4} = carbon tetrachloride solvate. RT (slow) – vial wrapped in Al foil, 8 °C (fast) – vial stored in refrigerator.

1.1.3. Antisolvent Addition Crystallisation

The antisolvent addition crystallisation screen was designed from 32 mixed solvent systems. **4-AQ** and solvents were dispensed at room temperature in various amounts, then filtered. Antisolvent was added drop-wise until either persistent clouding was observed or the maximum antisolvent volume (three times the volume of the solvent) was dispensed. Solid products were analysed with IR.

The results of the antisolvent addition crystallisation screen are summarised in Table S3. **MH** and **AH I°** were obtained as the crystallisation products.

Table S3. Summary of **4-AQ** antisolvent addition crystallisation experiments.

Solvent	Antisolvent	Solid Form[a]	Antisolvent	Solid Form[a]
Methanol	Toluene	○	Water	□
Ethanol	Toluene	□+○	Water	□
1-Propanol	Toluene	○	Water	□
2-Propanol	Toluene	□	Water	□
1-Butanol	Toluene	□	–	–
2-Butanol	Toluene	□	–	–
Acetone	Toluene	□	Water	□
Acetonitrile	Toluene	○	Water	□
Dimethyl formamide	Toluene	□	Water	□
Dimethyl sulfoxide	Toluene	□	Water	□
Dichloromethane	Toluene	○	–	–
Dichloroethane	Toluene	○	–	–
Chloroform	Toluene	○	–	–
Carbon tetrachloride	Toluene	○	–	–
Dioxane	Toluene	○	Water	□
Methyl acetate	Toluene	○	–	–
Ethyl acetate	Toluene	○	–	–
Diethyl ether	Toluene	○	–	–
Ethyl methyl ketone	Toluene	□+○	–	–
Nitromethane	Toluene	○	–	–
Pyridine	Toluene	□	–	–
Tetrahydrofurane	Toluene	○	Water	□

[a]□= MH , ○ = AH I°

1.1.4. Liquid Assisted Grinding (LAG) Experiments

15–20 mg of **4-AQ** and few drops of solvent were ground in a Retsch grinding mill MM301 for 10 minutes. The wet product was analysed with XRPD. The results are summarised in Table S4. Only **MH** and **AH I°** were obtained in the LAG experiments.

Table S4. Summary of **4-AQ** liquid assisted grinding experiments.

Solvent	Solid Form[a]	Solvent	Solid Form[a]
Methanol	□	Carbon tetrachloride	○
Ethanol	□+○	Dioxane	○
1-Propanol	○	Methyl acetate	○
2-Propanol	○	Ethyl acetate	○
1-Butanol	○	Diethyl ether	○
2-Butanol	○	Ethyl methyl ketone	○
1-Pentanol	○	Nitromethane	○
2-Pentanol	○	Pyridine	○
t-Pentanol	○	Tetrahydrofurane	○
Acetone	○	Toluene	○
Acetonitrile	○	Xylene	○
Dimethyl formamide	○	Heptane	○
Dimethyl sulfoxide	○	Water	□
Chloroform	○	–	–

[a]□= MH , ○ = AH I°

1.2 Characterisation of 4-AQ Anhydrates and Carbon Tetrachloride Solvate

1.2.1. Anhydrate I°

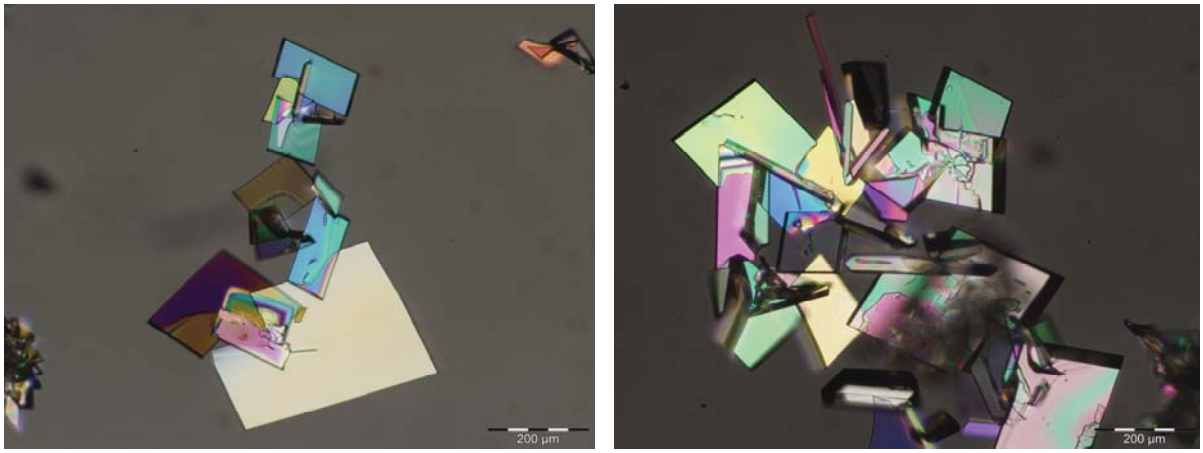

(a) 150 °C (after 15 minutes) (b) 150 °C (after 5 hours)

Figure S1. AH I° single crystals obtained from sublimation experiments.

1.2.2. Anhydrate II

Crystallised form melt – **AH II**(melt):

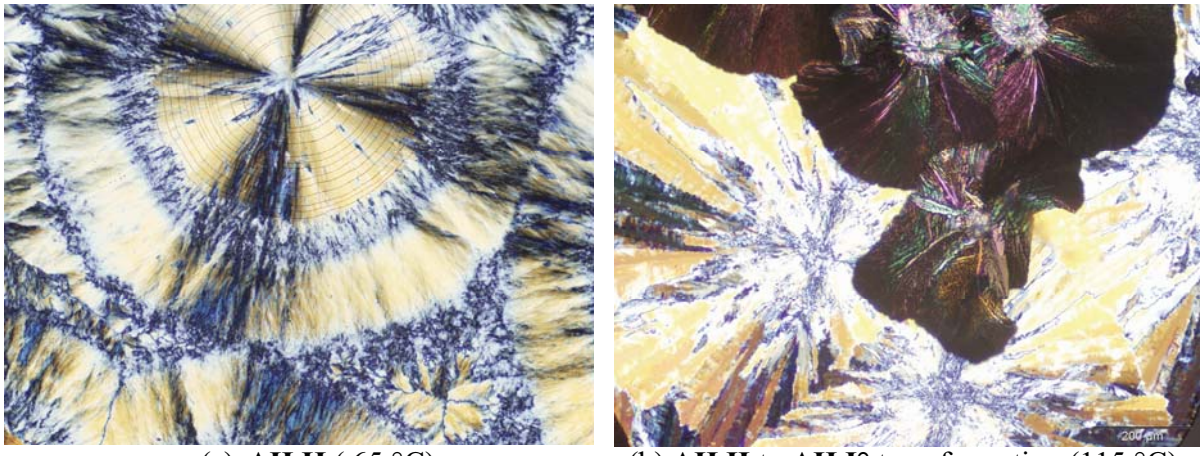

(a) **AH II** (65 °C) (b) **AH II** to **AH I°** transformation (115 °C)

Figure S2. Microphotographs showing (a) **AH II** and (b) the **AH II** to **AH I°** phase transformation.

The diffraction pattern of **AH II**(melt) (2θ: 2 – 45°, step size of 2θ = 0.007°) was indexed using the first twenty peaks with DICVOL04 and the space group was determined based on a statistical assessment of systematic absences,[1] as implemented in the DASH structure solution package.[2] Lattice parameters and space group corresponded to the computationally generated **AH II** structure (Fig. 8) ignoring temperature effects.

Pawley fits were performed with Topas Academic V5:[3] $R\bar{3}$, a = 28.422(9) Å, c = 11.967(5) Å (Figure S3). The background was modelled with Chebyshev polynomials and the modified Thompson-Cox-Hastings pseudo-Voigt (TCHZ) function was used for peak shape fitting.

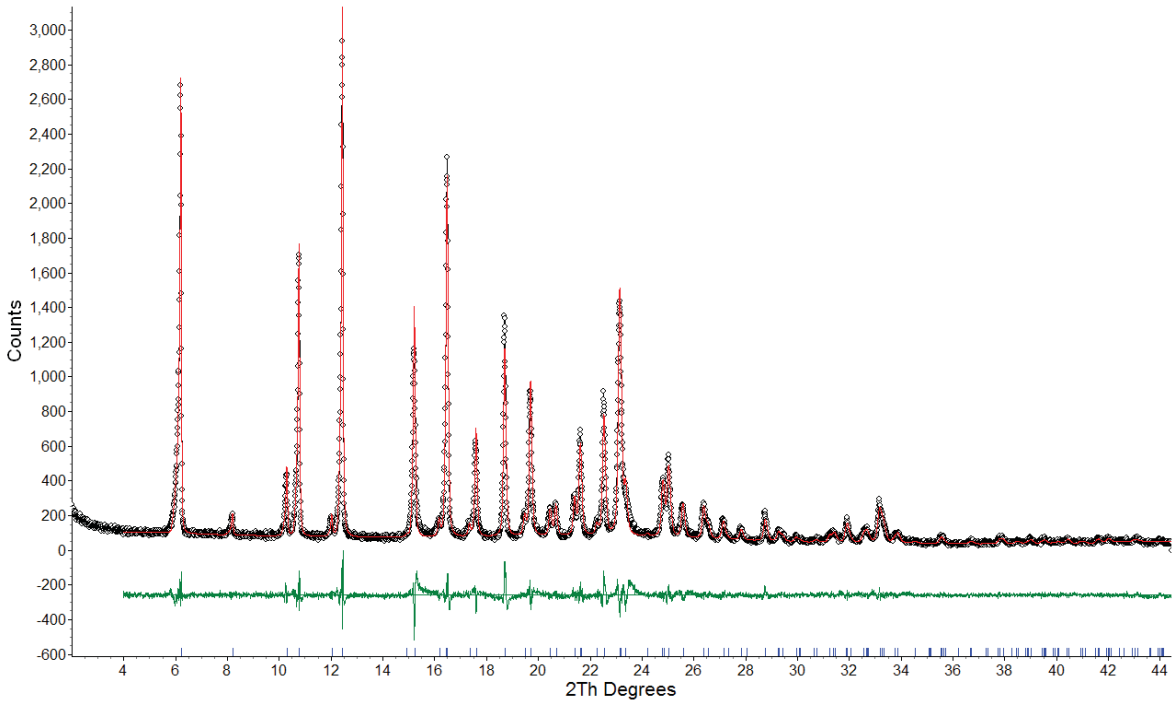

Figure S3. Pawley fit (R_{wp} = 12.32%, R_{exp} = 8.35%, R_p = 8.09%, gof = 1.48) between the reflection XRPD data of **AH II** (melt) with a model consisting of the cell parameters derived from the computationally generated **AH II** structure (Fig. 8). Black dots indicate raw data, while the red line indicates the calculated model. Tick marks (blue) are the 2θ positions for the hkl reflections. The difference pattern is shown in green.

Evaporation from Carbon Tetrachloride – **AH II**(CCl_4):

The diffraction pattern of **AH II** obtained from CCl_4 indexed[1,2] to $R\bar{3}$, a = 28.483(3) Å, c = 12.002(1) Å (Figure S4). In contrast to AH II(melt) the AH II(CCl_4) cell volume is increased by 0.7%, which can be related to the solvent molecules entrapped in the crystal lattice.

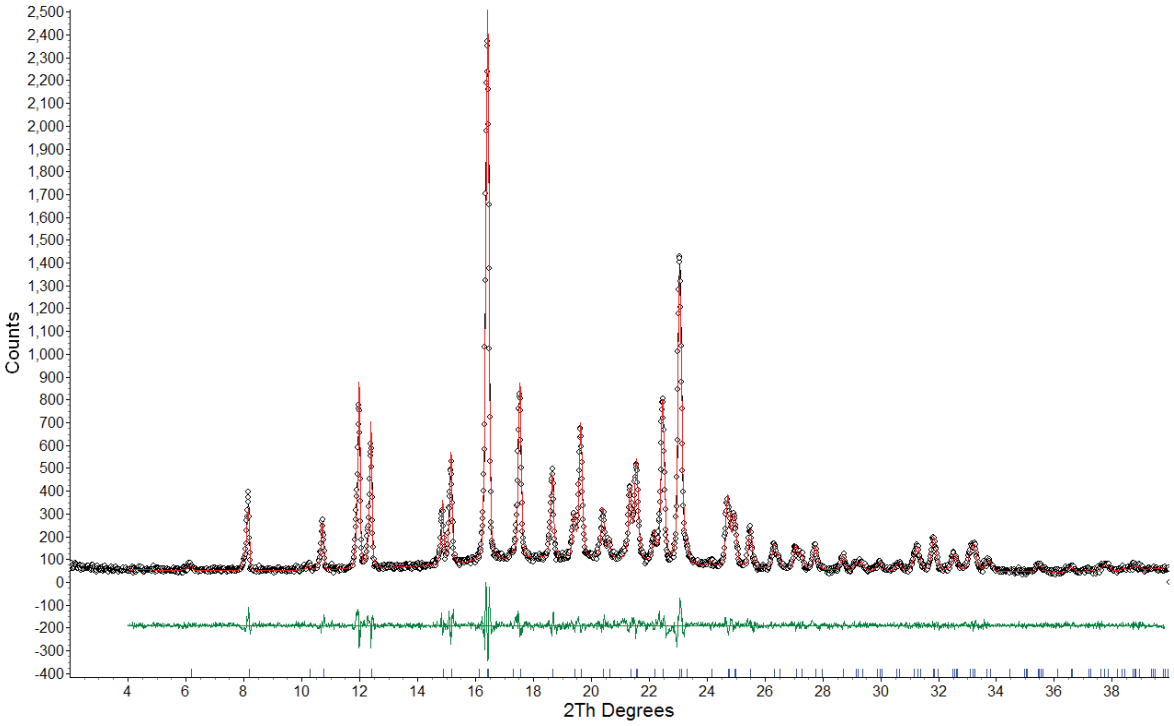

Figure S4. Pawley fit (R_{wp} = 9.33%, R_{exp} = 8.73%, R_p = 7.27%, *gof* = 1.07) between the reflection XRPD data of **AH II** (CCl_4) with a model consisting of the cell parameters derived from the single crystal structure **AH II**(CCl_4). Black dots indicate raw data, while the red line indicates the calculated model. Tick marks (blue) are the 2θ positions for the hkl reflections. The difference pattern is shown in green.

Evaporation from Chloroform – **AH II**($CHCl_3$):

Room temeprature evaporation of a at room temperature saturated **4-AQ** solution in chloroform resulted in a mixed phase, i.e. **AH I°** and **AH II**($CHCl_3$). All attempts to enrichen **AH II**($CHCl_3$) failed.

Evaporation from 1-Butanol – **AH II**(1BuOH):

Slow evaporation of an under-saturated solution of **4-AQ** in 1-butanol at 40 °C (solution saturated at RT) lead to **AH II**(1BuOH) or a mixture of **AH II**(1BuOH) and **AH I°**. Pawley fit, using the cell parameters derived for **AH II**(CCl_4) as starting point, is given in Figure S5 ($R\bar{3}$, a = 28.4449(8) Å, c = 11.990(15) Å).

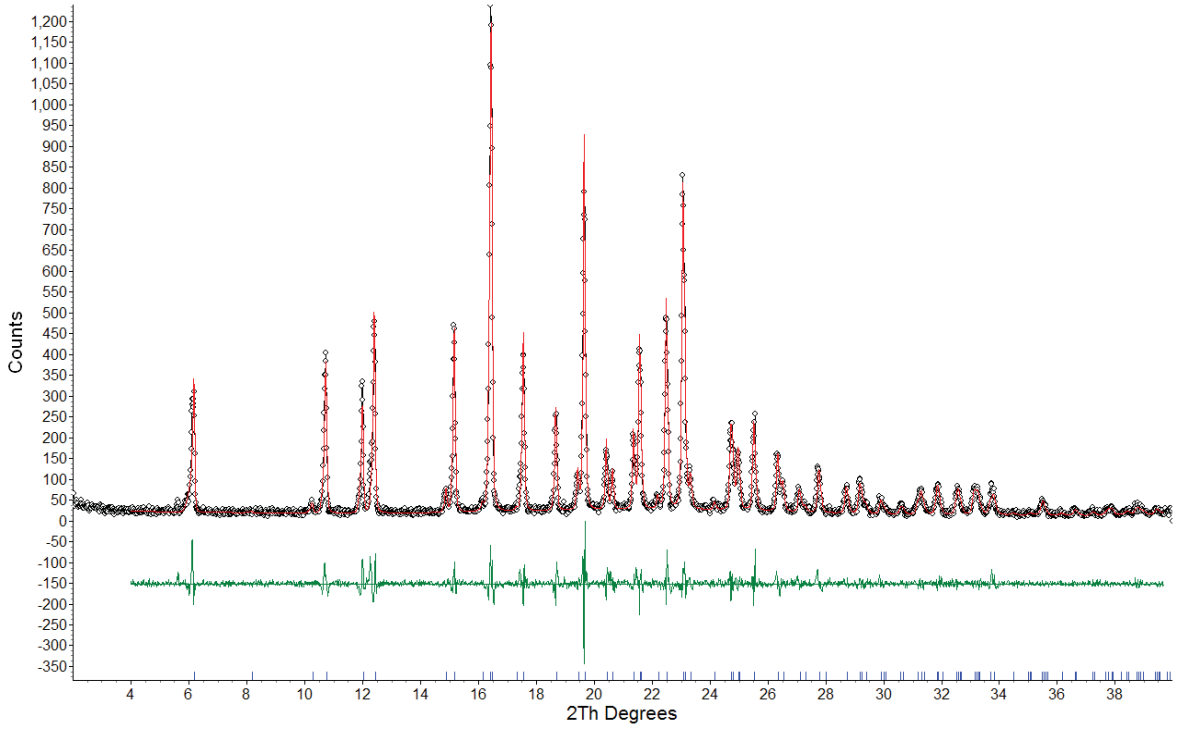

Figure S5. Pawley fit (R_{wp} = 15.06%, R_{exp} = 13.23%, R_p = 11.34%, *gof* = 1.14) between the reflection XRPD data of **AH II** (1BuOH) with a model consisting of the cell parameters derived from the single crystal structure **AH II**(CCl_4). Black dots indicate raw data, while the red line indicates the calculated model. Tick marks (blue) are the 2θ positions for the hkl reflections. The difference pattern is shown in green.

Evaporation from Tetrahydrofuran – **AH II**(THF):

Evaporation of **4-AQ** from THF at 40 °C, using a at RT saturated solution, lead to **AH II**(THF) and **AH I°**. It was not possible to produce phase pure **AH II**(THF). A subset of the XPRD patterns given in Fig. 3 is shown enlarged in Figure S6.

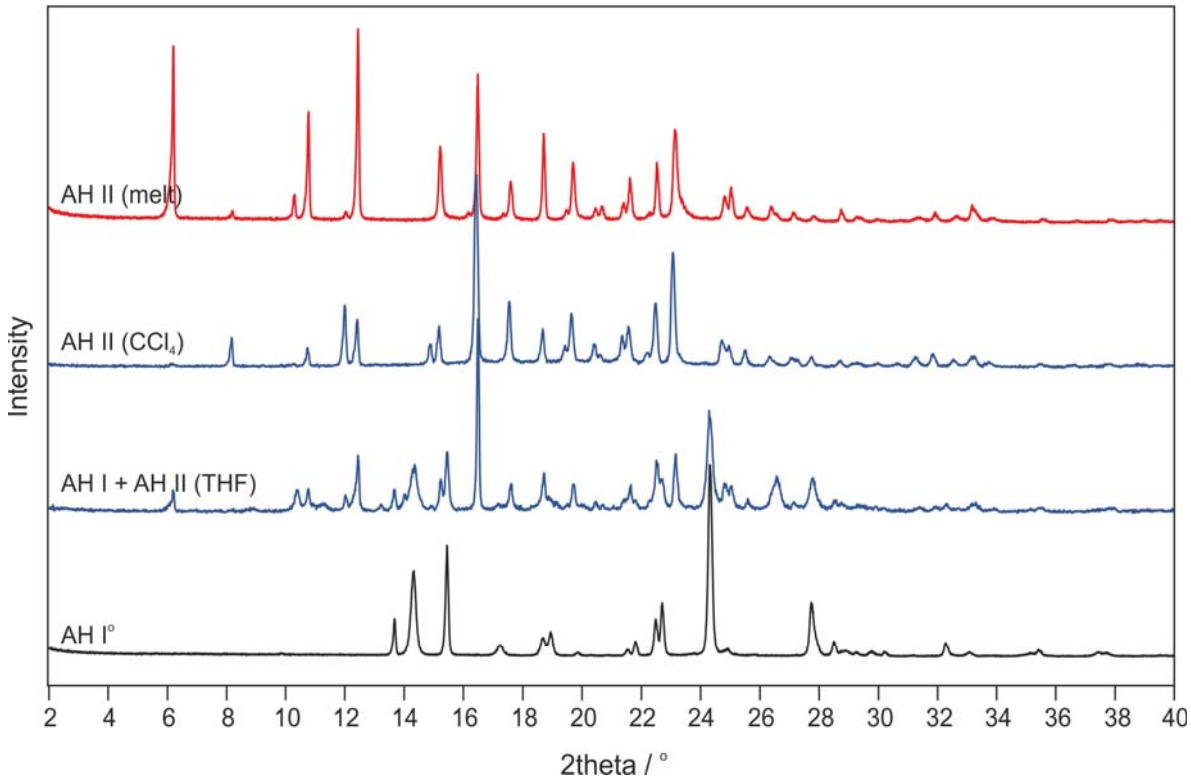

Figure S6. Comparison of XRPD patterns of **AH II**(melt), **AH II**(CCl_4), mixture of **AH II**(THF) + **AH I°** and **AH I°**.

1.2.3. Anhydrate III

The **AH III** XRPD pattern was successfully indexed (Figure S7, Table S7): $R\bar{3}$, a = 31.511(5) Å, c = 4.666(1) Å. It has to be noted that the **AH III** samples always showed traces of **AH I°**. The **AH III** lattice parameters determined at RT match the parameters of one of the computationally generated low energy structures, if temperature effects are ignored (structure 4_10, Table S6).

The **AH III** IR spectrum (Fig. 2a) indicates the presence of a Z′=1 structure, in agreement with the computationally generated structure 4_10.

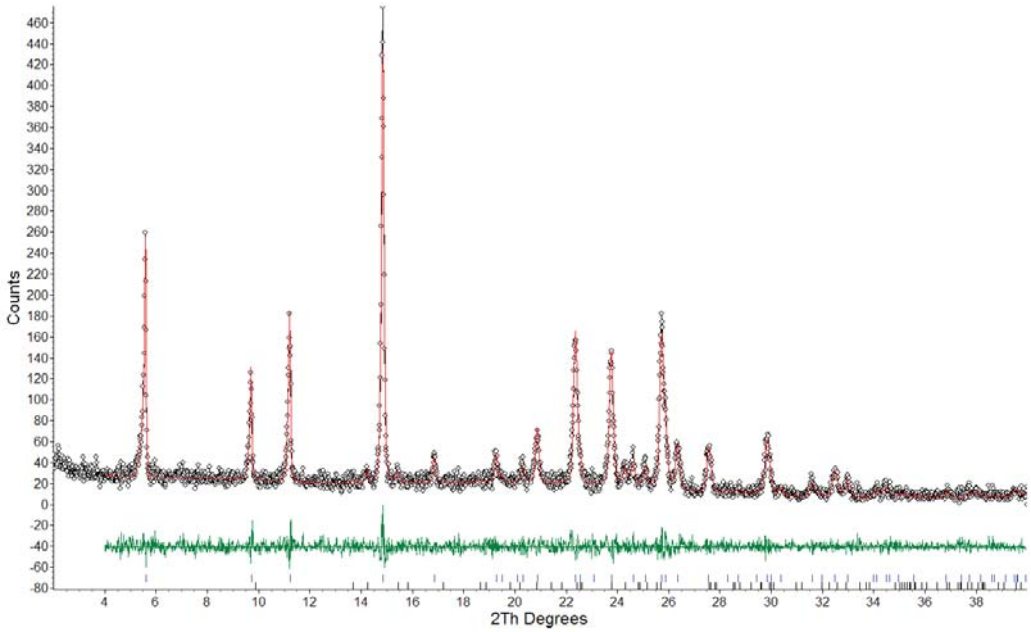

Figure S7. Pawley fit (R_{wp} = 16.54%, R_{exp} = 18.74%, R_p = 12.11%, *gof* = 0.88) between the reflection XRPD data of **AH III**/**AH I°** with a model consisting of the cell parameters derived from the computationally generated structure for **AH III** and the single crystal structure **AH I°**. Black dots indicate the raw data, while the red line indicates the calculated model. Tick marks (blue) are the 2θ positions for the hkl reflections. The difference pattern is shown in green.

1.2.3. Carbon Tetrachloride Solvate

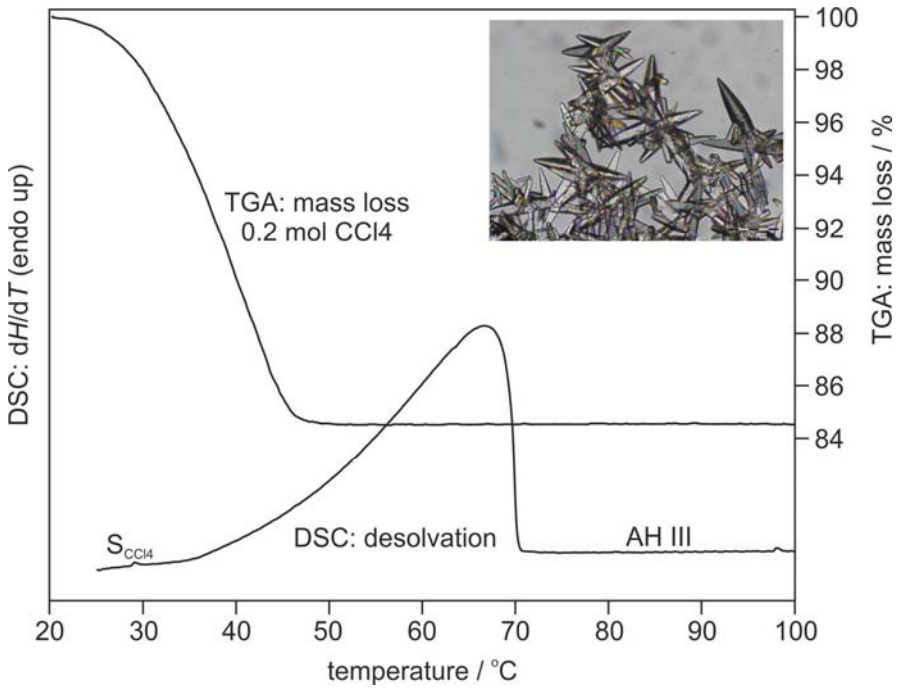

Figure S8. DSC and TGA thermograms of **4-AQ S_{CCl4}**. Photograph shows S_{CCl4} crystals in solution.

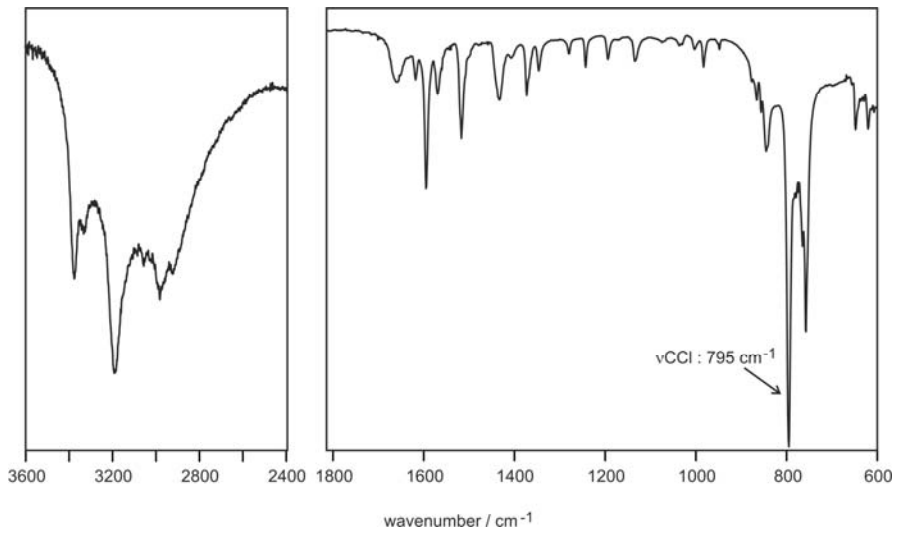

Figure S9. FT-IR spectra of **4-AQ S_{CCl4}** (recorded on a ZnSe ATR crystal on a Perkin Elmer Spectrum GX Fourier Transform spectrophotometer (Perkin Elmer, Norwalk Ct., USA) over a range of 4000 to 600 cm^{-1} with a resolution of 2 cm^{-1} (24 scans)).

1.3 Thermodynamic Stability - Semi-schematic Energy/Temperature Diagram

The thermodynamic relationship of the **4-AQ** anhydrate polymorphs is displayed in a semi-schematic energy/temperature diagram (Figure S10). Polymorphic pairs **AH I°/II** and **AH I°/III** show a monotropic relationship.

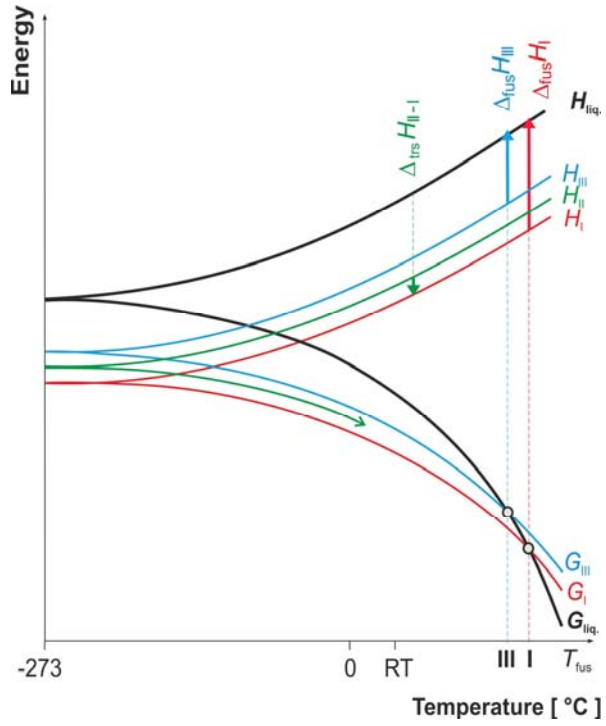

Figure S10. Semi-schematic energy/temperature diagram of **4-AQ** anhydrate polymorphs. T_{fus} = melting point, G = Gibbs free energy, H = enthalpy, $\Delta_{fus}H$ = enthalpy of fusion, $\Delta_{trs}H$ = transition enthalpy, liq. $\Delta_{fus}H$ =liquid phase (melt).

2 Computational Search for Anhydrate Polymorphs

2.1 Conformational Analysis of 4-Amino-2-methylquinoline

The potential energy surface scan of the **4-AQ** C3–C2–N2–H1 torsion (Figure 1), given in Figure S11, shows that there are two identical minima, separated by a significant barrier of ca. 45 kJ mol^{-1} (calculated at the PBE0/6-31G(d,p) level of theory). In the conformational energy minimum, with the amino group modelled as planar (as opposed to pyramidal), the polar hydrogen atoms are in plane with the quinolone ring (ϕ_1 = 0, 180, 360 °). The amino group can move ± 30 ° for less than 10 kJ mol^{-1}. In the experimental anhydrate structures (**AH I°** and **AH II**) the amino groups deviate slightly form planarity (slightly pyramidal) but are still closely related to the (planar) conformation energy minimum, as observed in the monohydrate (LOBSOL[4]). The energy difference between the planar and pyramidal minima was calculated as 2.6 kJ mol^{-1} (PBE0/6-31G(d,p)).

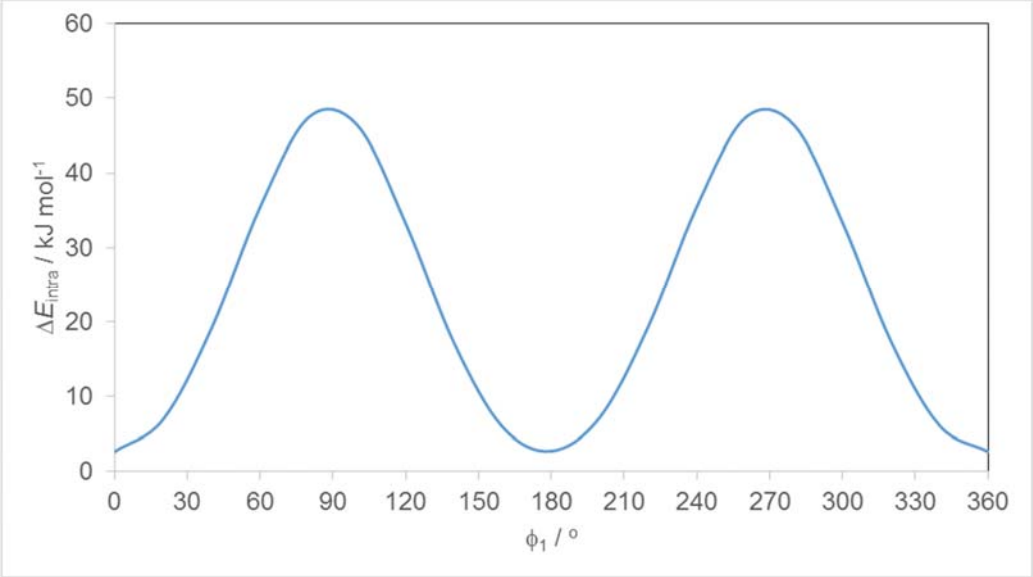

Figure S11. Conformational energy scan of ϕ_1 (C3−C2−N2−H1) for an isolated **4-AQ** molecule at PBE0/6-31G(d,p) level of theory. The amino group was modelled as planar and the rest of the molecule was optimised at each value of ϕ_1, which was calculated every 20 °.

2.2 Computational Generation of the Crystal Energy Landscape

2.2.1. Space groups

Z'=1 anhydrate structures were randomly generated in following 48 space groups, $P1$, $P\bar{1}$, $P2_1$, $P2_1/c$, $P2_12_12$, $P2_12_12_1$, $Pna2_1$, $Pca2_1$, $Pbca$, $Pbcn$, $C2/c$, Cc, $C2$, Pc, Cm, $P2_1/m$, $C2/m$, $P2/c$, $C222_1$, $Pmn2_1$, $Fdd2$, $Pnna$, $Pccn$, $Pbcm$, $Pnnm$, $Pmmn$, $Pnma$, $P4_1$, $P4_3$, $I\bar{4}$, $P4/n$, $P4_2/n$, $I4/m$, $I41/a$, $P41212$, $P4_32_12$, $P3_1$, $P3_2$, $R3$, $P\bar{3}$, $R\bar{3}$, $P3_121$, $P3_22_1$, $R3c$, $R\bar{3}c$, $P6_1$, $P6_3$, $P6_3/m$.

2.2.2. DFT-D Calculations: Methodology

The DFT-D calculations were carried out with the CASTEP plane wave code[5] using the Perdew-Burke-Ernzerhof (PBE) generalised gradient approximation (GGA) exchange-correlation density functional[6] and ultrasoft pseudopotentials,[7] with the addition of a semi-empirical dispersion correction, either the Tkatchenko and Scheffler (TS) model,[8] or Grimme06 (G06) .[9] In a first step, the structures were geometry optimised using the TS dispersion correction. Brillouin zone integrations were performed on a symmetrised Monkhorst–Pack *k*-point grid with the number of *k*-points chosen to provide a maximum spacing of 0.07 $Å^{-1}$ and a basis set cut-off of 560 eV. The self-consistent field convergence on total energy was set to $1x10^{-5}$ eV. Energy minimisations were performed using the Broyden–Fletcher–Goldfarb–Shanno optimisation scheme within the space group constraints. The optimisations were considered complete when energies were converged to better than $2x10^{-5}$ eV per atom, atomic displacements converged to $1x10^{-3}$ Å, maximum forces to $5x10^{-2}$ eV $Å^{-1}$, and maximum stresses were converged to $1x10^{-1}$ GPa. Energy minimisations with variable unit cells were restarted after the first minimisation to reduce the effects of changes in unit cell on the basis set. The energies for all anhydrates within 15 kJ mol^{-1} of the lowest structure were recalculated, without optimisation, with the number of *k*-points chosen to provide a maximum spacing of 0.04 $Å^{-1}$ and a basis set cut-off of 780 eV, using the G06 dispersion correction, resulting in the final crystal energy landscape (Fig. 8). Isolated molecule minimisations to compute the isolated **4-AQ** energy (U_{gas}) were performed by placing a single molecule in a fixed cubic 35x35x35 $Å^3$ unit cell and optimised and recalculated with the same settings used for the crystal calculations.

2.2.3. Lowest Energy Structures (CrystalOptimizer and PBE-D)

All calculated structures are available in .res format from the authors on request. The lowest energy structures derived from CryOpt and DFT-D (PBE-TS/PBE-G06) calculations are given in Table S5 and Table S6, respectively.

Table S5. Hypothetical and known low-energy crystal structures of **4-AQ** (CryOpt).

Str. ID[a]	Z'	Space group	Cell parameters						E_{latt}/ kJ mol^{-1}	ΔE_{latt}/ kJ mol^{-1}	Density g cm^{-3}
			a/Å	b/Å	c/Å	α/°	β/°	γ/°			
10 (III)	1	$R\bar{3}$	31.556	31.556	4.544	90	90	120	–110.31	0.00	1.207
160 (I)	1	$P2_1/c$	5.147	12.565	12.977	90	97.94	90	–110.28	0.03	1.264
157	1	$P2_1/c$	4.791	14.306	13.500	90	115.30	90	–109.69	0.62	1.256
8	1	$P2_1/c$	5.246	13.343	12.512	90	107.88	90	–109.30	1.00	1.260
67	1	$R\bar{3}$	31.628	31.628	4.570	90	90	120	–107.79	2.52	1.194
2	1	$Pna2_1$	12.986	13.231	4.837	90	90	90	–107.18	3.13	1.264
152	1	*Pbca*	12.972	10.240	12.807	90	90	90	–106.44	3.87	1.235
16	1	$Pna2_1$	17.116	12.164	4.075	90	90	90	–106.21	4.10	1.239
158	1	*Cc*	4.791	14.583	12.400	90	95.92	90	–105.97	4.34	1.220
122	1	$Pna2_1$	15.098	12.016	4.609	90	90	90	–105.41	4.89	1.257
48	1	*Fdd*2	24.726	26.059	5.370	90	90	90	–105.13	5.17	1.215
110	1	*R*-3	31.848	31.848	4.628	90	90	120	–105.11	5.20	1.163
35	1	*Fdd*2	35.342	24.780	3.961	90	90	90	–105.10	5.21	1.212
137	1	*Pbca*	10.180	13.111	13.010	90	90	90	–105.03	5.28	1.210
19	1	$P2_1/c$	4.004	17.461	13.893	90	63.01	90	–104.94	5.36	1.214
98	1	$P2_1/c$	13.195	5.6528	12.018	90	71.19	90	–104.88	5.42	1.238
295	1	$P2_1/c$	3.984	17.509	12.506	90	82.31	90	–104.86	5.45	1.215
1026	1	$P2_1/c$	13.116	5.872	13.678	90	54.27	90	–104.83	5.47	1.229
170	1	*R*-3	24.974	24.974	8.052	90	90	120	–104.71	5.60	1.087
95	1	*Fdd*2	25.285	27.982	4.901	90	90	90	–104.45	5.86	1.212
75	1	*Cc*	12.918	12.049	5.776	90	75.15	90	–103.83	6.48	1.209
640	1	$P2_1/c$	13.026	6.151	10.834	90	93.44	90	–103.50	6.81	1.213
32	1	$\bar{3}R$	32.963	32.963	4.240	90	90	120	–103.38	6.93	1.185
229	1	$Pna2_1$	15.216	4.772	11.880	90	90	90	–103.36	6.95	1.218
2502	1	$Pna2_1$	15.074	11.886	4.797	90	90	90	–103.12	7.19	1.223
187	1	*Pbca*	5.733	13.249	22.731	90	90	90	–103.06	7.25	1.217
1012	1	*Pbca*	22.111	6.087	13.030	90	90	90	–102.90	7.40	1.198
111	1	$P2_1/c$	4.205	16.764	12.539	90	85.57	90	–102.66	7.64	1.193
99	1	*Pbca*	11.503	11.711	13.043	90	90	90	–102.52	7.79	1.196
159	1	$P2_1/c$	12.977	5.465	12.676	90	72.56	90	–102.36	7.95	1.225
224	1	*C*2/*c*	27.324	4.926	12.744	90	83.53	90	–102.32	7.99	1.233
1019	1	$Pna2_1$	12.392	17.066	4.109	90	90	90	–102.04	8.26	1.209
91	1	*Fdd*2	35.744	24.829	4.056	90	90	90	–102.02	8.29	1.168
22	1	$P2_1/c$	4.311	16.578	12.384	90	82.00	90	–102.01	8.29	1.199
570	1	*Cc*	13.548	6.114	13.066	90	125.12	90	–102.01	8.29	1.187
228	1	$P2_1/c$	13.859	4.876	12.816	90	92.77	90	–102.01	8.30	1.215
162	2	$R\bar{3}$	31.224	31.224	9.953	90	90	120	–101.92	8.39	1.125
139	1	*C*2/*c*	16.335	11.456	12.218	90	51.64	90	–101.90	8.40	1.172
162	1	*Pccn*	16.931	7.950	12.790	90	90	90	–101.88	8.43	1.221
317	1	$P2_12_12_1$	4.480	12.869	14.042	90	90	90	–101.85	8.46	1.298
134	1	$P2_1/c$	13.321	5.186	12.565	90	90	90	–101.71	8.59	1.292
127	1	$Pna2_1$	10.812	10.931	7.270	90	90	90	–101.71	8.60	1.223

Str. ID[a]	Z'	Space group	Cell parameters						E_{latt}/ kJ mol^{-1}	ΔE_{latt}/ kJ mol^{-1}	Density g cm^{-3}
			a/Å	b/Å	c/Å	α/°	β/°	γ/°			
685	1	$P2_1/c$	8.470	9.794	10.645	90	77.79	90	–101.59	8.72	1.217
135	1	$Pna2_1$	13.350	13.926	4.658	90	90	90	–101.58	8.72	1.213
282	1	$P2_1/c$	10.104	9.161	9.731	90	77.31	90	–101.51	8.80	1.196
9 (II)	2	$R\bar{3}$	28.002	28.002	12.281	90	90	120	–101.49	8.82	1.134
142	1	$Pccn$	8.052	16.899	12.766	90	90	90	–101.48	8.83	1.210
88	1	$Fdd2$	24.814	35.289	4.028	90	90	90	–101.41	8.90	1.192
80	1	$P2_1/c$	11.903	6.289	12.120	90	110.01	90	–101.40	8.90	1.233
1224	1	$Pna2_1$	12.980	6.303	10.821	90	90	90	–101.17	9.14	1.187
24	1	$Pca2_1$	15.538	4.675	11.856	90	90	90	–101.04	9.27	1.220
73	1	$P2_1/c$	5.873	12.644	11.962	90	76.06	90	–101.04	9.27	1.219
472	1	$C2/c$	21.508	6.695	12.891	90	109.97	90	–100.94	9.36	1.205
97	1	$Pca2_1$	13.397	4.995	13.174	90	90	90	–100.89	9.42	1.192
356	1	$Fdd2$	5.671	25.418	24.421	90	90	90	–100.80	9.51	1.194
1113	1	$Fdd2$	29.223	25.543	4.718	90	90	90	–100.65	9.65	1.194
2505	1	$Pna2_1$	13.321	5.186	12.565	90	90	90	–100.63	9.67	1.211
1487	1	$P2_1$	13.840	4.902	8.209	90	48.52	90	–100.50	9.81	1.259
561	1	Cc	28.838	4.983	12.834	90	67.40	90	–100.49	9.81	1.185
150	1	$Pbcn$	14.673	12.995	9.201	90	90	90	–100.38	9.92	1.198
133	1	$Pna2_1$	13.100	6.014	11.284	90	90	90	–100.32	9.99	1.182

[a]Structure ID corresponds to the CrystalPredictor ranking. I – **AH I°**, II – **AH II**, III – **AH III**.

Table S6. Hypothetical and known low-energy crystal structures of **4-AQ** (PBE-TS and **PBE-G06, Fig. 8**).

Str. ID[a]	exptl.	Space group	Cell parameters						PBE-TS[b]		PBE-G06[c]		PI[d]/ %	Void Space[e] (%/Å^3)
			a/Å	b/Å	c/Å	α/°	β/°	γ/°	E_{latt}/ kJ mol^{-1}	ΔE_{latt}/ kJ mol^{-1}	E_{latt}/ kJ mol^{-1}	ΔE_{latt}/ kJ mol^{-1}		
1_160	I	$P2_1/c$	5.058	12.090	12.992	90	97.97	90	–154.93	0.00	**–132.18**	**0.00**	75.6	0/0
2_9	II	$R\bar{3}$	27.996	27.996	11.640	90	90	120	–144.83	10.09	**–129.00**	**3.18**	67.4	6.3/499.38
3_640		$P2_1/c$	9.996	9.390	12.974	90	99.42	90	–145.74	9.19	**–128.18**	**4.00**	72.6	2.3/0.1
4_10	III	$R\bar{3}$	31.265	31.265	4.425	90	90	120	–149.83	5.10	**–127.35**	**4.83**	71.5	7.2/271.09
5_157		$P2_1/n$	4.677	14.017	12.268	90	94.88	90	–148.83	6.10	**–126.96**	**5.22**	74.3	0/0
6_16		$Pna2_1$	16.724	12.106	3.894	90	90	90	–149.27	5.65	**–126.77**	**5.41**	75.4	1.4/10.98
7_75		Ic	5.688	11.248	12.703	90	98.86	90	–147.09	7.85	**–125.67**	**6.51**	73.9	0/0
8_152		$Pbca$	9.872	12.558	12.979	90	90	90	–146.95	7.98	**–125.62**	**6.55**	73.9	0/0
9_134		$P2_1/c$	3.975	12.119	15.994	90	95.27	90	–148.81	6.12	**–124.64**	**7.54**	77.5	0/0
10_8		$P2_1/n$	4.858	13.834	12.075	90	94.50	90	–147.85	7.08	**–124.45**	**7.73**	73.8	0/0
11_2		$Pna2_1$	12.984	12.883	4.776	90	90	90	–147.91	6.10	**–124.32**	**7.86**	74.6	0/0
12_1012		$Pbca$	6.129	13.067	20.835	90	90	90	–141.35	13.58	**–124.10**	**8.08**	71.1	1.0/16.39
13_122		$Pna2_1$	14.771	12.106	4.451	90	90	90	–145.82	9.11	**–123.84**	**8.34**	74.7	0/0
14_1026		$P2_1/c$	11.722	5.954	13.175	90	115.89	90	–142.43	12.50	**–123.80**	**8.38**	71.9	0/0
15_80		$P2_1/c$	11.509	6.286	12.089	90	111.68	90	–142.57	12.36	**–122.98**	**9.20**	73.1	0/0
16_561		Ic	9.674	6.572	13.049	90	92.34	90	–140.00	14.93	**–122.76**	**9.42**	71.8	0/0
17_98		$P2_1/c$	11.600	5.657	13.252	90	110.38	90	–142.82	12.11	**–122.70**	**9.48**	72.9	0/0
18_187		$Pbca$	5.616	13.392	21.988	90	90	90	–140.32	14.61	**–122.63**	**9.54**	71.9	0/0
19_35		$Fdd2$	24.569	34.794	3.794	90	90	90	–145.56	9.37	**–122.50**	**9.68**	73.5	4.4/143.17
20_97		$Pca2_1$	12.962	4.773	13.156	90	90	90	–142.55	12.37	**–121.97**	**10.21**	73	0/0
21_137		$Pbca$	9.816	12.742	13.137	90	90	90	–140.96	13.97	**–121.88**	**10.30**	72.4	3.3/54.23
22_19		$P2_1/c$	3.801	17.414	12.360	90	97.55	90	–144.95	9.98	**–121.55**	**10.63**	73.4	4.3/39.98
23_472		$I2/a$	12.919	6.588	20.237	90	105.18	90	–139.46	15.47	**–121.44**	**10.74**	71.6	2.4/40.56
24_110		$R\bar{3}$	31.613	31.613	4.477	90	90	120	–140.97	13.96	**–121.15**	**11.03**	69.2	6.7/258.33
25_229		$Pna2_1$	14.877	4.593	11.987	90	90	90	–141.95	12.98	**–120.98**	**11.20**	72.7	0/0

[a]Structure ID: rank PBE-G06_rank CrystalPredictor. [b]Structure optimised (see section 2.2.2). [c]Single point energies using the PBE-TS structures. I – **AH I°**, II – **AH II**, III – **AH III**. [d]PI - Kitaigorodskii type of packing index, calculated using PLATON.[10] [e]Void space was calculated using a 1.0 Å probe radius and an approx. grid spacing of 0.1 Å and is given as % of unit cell volume and in Å^3.

2.3 Representation of the Experimental Structures

The computational models were successful in reproducing the experimental structures (Table S7). The computationally generated low energy structures were compared using the Packing similarity tool in the Solid Form module of Mercury to determine the root mean square deviation of the non-hydrogen atoms in a cluster of 15 molecules ($rmsd_{15}$).[11]

Table S7. Quality of representation of the CryOpt (CrystalOptimizer) and PBE-D anhydrate structures.

	Lattice parameters (cell vectors/Å, angles/°)						cell volume	$rmsd_{15}$
	a	*b*	*c*	α	β	γ	(Å^3)	(Å)
AH I (exp.) , $P2_1/c$, 293 K[a]	5.216	12.369	13.119	90	99.07	90	835.81	–
AH I (CryOpt) , $P2_1/c$, 0 K	5.147	12.565	12.977	90	97.94	90	831.20	0.26
AH I (PBE-D) , $P2_1/c$, 0 K	5.058	12.090	12.992	90	97.97	90	786.80	0.22
AH II (exp, melt), $R\bar{3}$, 298 K[b]	28.422	28.422	11.967	90	90	120	8372.91	–
AH II (exp, THF), $R\bar{3}$, 298 K[b]	28.389	28.389	11.946	90	90	120	8337.82	–
AH II (exp, 1BuOH), $R\bar{3}$, 298 K[b]	28.449	28.449	11.990	90	90	120	8403.94	–
AH II (exp, CCl_4), $R\bar{3}$, 298 K[b]	28.483	28.483	12.002	90	90	120	8432.47	–
AH II (exp., CCl_4), $R\bar{3}$, 173 K[a]	28.397	28.397	11.924	90	90	120	8327.16	–
AH II (CryOpt), $R\bar{3}$, 0 K	28.002	28.002	12.281	90	90	120	8339.53	0.32
AH II (PBE-D), $R\bar{3}$, 0 K	27.996	27.996	11.640	90	90	120	7900.87	0.19
AH III (exp), $R\bar{3}$, 298 K[b]	31.511	31.511	4.666	90	90	120	4012.35	–
AH III (CryOpt), $R\bar{3}$, 0 K	31.556	31.556	4.544	90	90	120	3918.61	–
AH III (PBE-D), $R\bar{3}$, 0 K	31.265	31.265	4.425	90	90	120	3745.93	–

[a]Single crystal structure, [b]lattice parameters derived from Pawley fits.

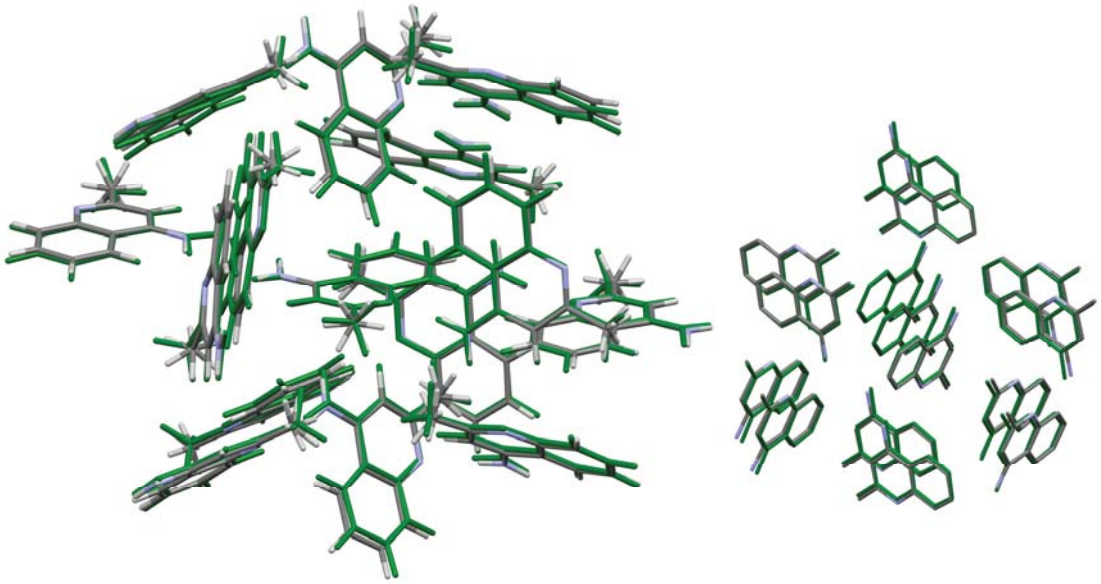

Figure S12. Overlay of the 15 molecule cluster of the observed structure of **AH I°** (coloured by element) and calculated PBE-D structure (green), $rmsd_{15}$=0.22 Å; left: including protons, right: without protons.

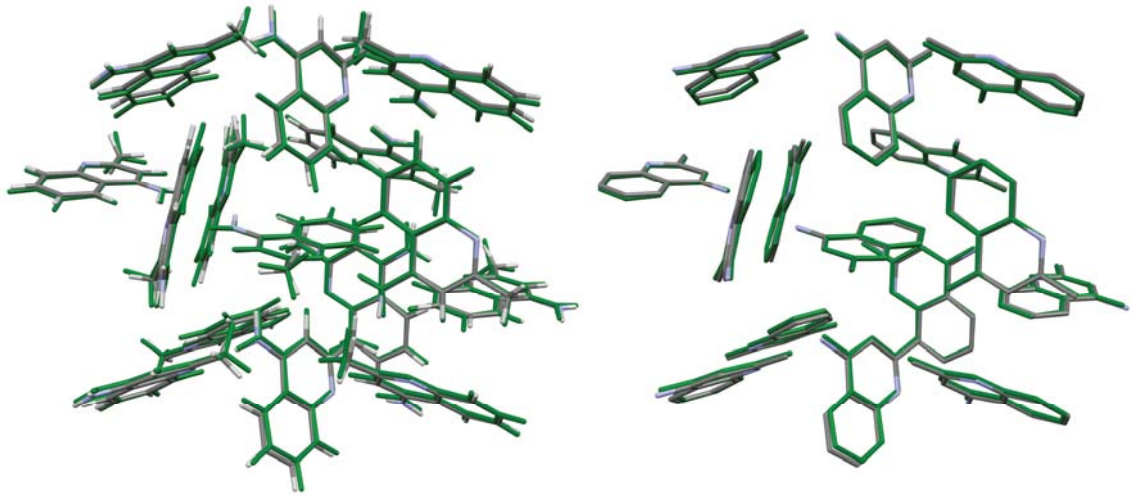

Figure S13. Overlay of the 15 molecule cluster of the observed structure of **AH II** (coloured by element) and calculated PBE-D structure (green), $rmsd_{15}$=0.19 Å; left: including protons, right: without protons.

2.4 PIXEL Calculations

PIXEL energies are intermolecular energies (i.e. U_{inter}) derived by integration over the isolated molecule charge densities placed in the crystal structures. The electrostatic contribution E_C is rigorously derived by this procedure and various approximations are used to estimate the polarisation (induction) E_P, dispersion E_D, and repulsion E_R contribution to the intermolecular lattice energy. The calculations also provide an approximate breakdown into contributions from different pairs of molecules in the coordination shell.

It has to be noted that the non-additivity of the molecule···molecule polarisation energies could not be taken into account for calculating the dimeric energies given in Table S8. This error was estimated by considering the lattice energies obtained by summing the molecule···molecule pairwise energies. These energies differ from the PIXEL lattice energies when the polarisation is calculated from the net field (i.e. accounting for non-additivity of the electrostatic field around a molecule) by approximately a max. ± 2.5% error in lattice energy. Thus the neglect of non-additivity and distant interactions does not qualitatively affect the results in the m/s.

Table S8. PIXEL calculations on **4-AQ** lowest energy structures (**AH I°**, **AH II**, **3**, **AH III, 5** and **6**). Only the most relevant intermolecular interactions for pairs of molecules are listed.

Structure	Interaction[a]	E_C[b]	E_P[c]	E_D[d]	E_R[e]	U_{inter}[f]
		kJ mol^{-1}				
AH I°	N–H···N (6.497)	–62.5	–29.4	–31.4	76.4	–46.9
$P2_1/c$	π···π (5.058)	–0.2	–3.7	–32.5	19.0	–17.4
	C–H···π (6.789)	–9.7	–4.8	–19.7	17.6	–16.6
AH II	N–H···N (6.319)	–57.6	–24.9	–31.2	67.4	–49.0
$R\bar{3}$	N–H···N (6.112)	–68.5	–31.9	–35.1	86.8	–48.7
	N–H···N (5.507)	–35.0	–17.1	–34.8	47.4	–39.5
	C–H···π (5.783)	–12.7	–10.7	–30.9	30.0	–24.3
	C–H···π (5.885)	–9.4	–5.9	–29.3	29.7	–14.9
3	N–H···N (6.490)	–65.0	–30.0	–35.6	84.9	–45.9
$P2_1/c$	C–H···π (7.405)	–5.2	–2.2	–11.1	2.7	–15.9
AH III	N–H···N (6.681)	–63.0	–29.3	–31.9	80.5	–43.7
$R\bar{3}$	π···π (4.425)	–2.9	–5.7	–45.3	33.0	–20.8
5	N–H···N (6.380)	–74.0	–36.1	–38.3	104.4	–43.9
$P2_1/n$	π···π (4.677)	–3.6	–6.5	–41.7	34.2	–17.7
6	N–H···N (6.844)	–56.1	–25.3	–27.3	70.2	–38.5
$Pna2_1$	π···π (3.894)	–5.2	–8.8	–50.4	45.1	–19.2
	N/C–H···C (6.741)	–9.7	–5.9	–21.9	21.6	–15.9

[a]PIXEL energies are for a pair of molecules. The pairs of molecules are defined by the strongest intermolecular interaction and distance between their centres of mass in Å; [b]electrostatic (Coulombic) energy; [c]polarisation energy; [d]dispersion energy; [e]repulsion energy; [f]total intermolecular energy: $U_{inter} = E_C + E_P + E_D + E_R$. The non-additivity of E_P is not included.

2.5 Hirshfeld Surfaces

For the generation of the Hirshfeld 2D fingerprint plots the structures on Fig. 8 were used as input files.

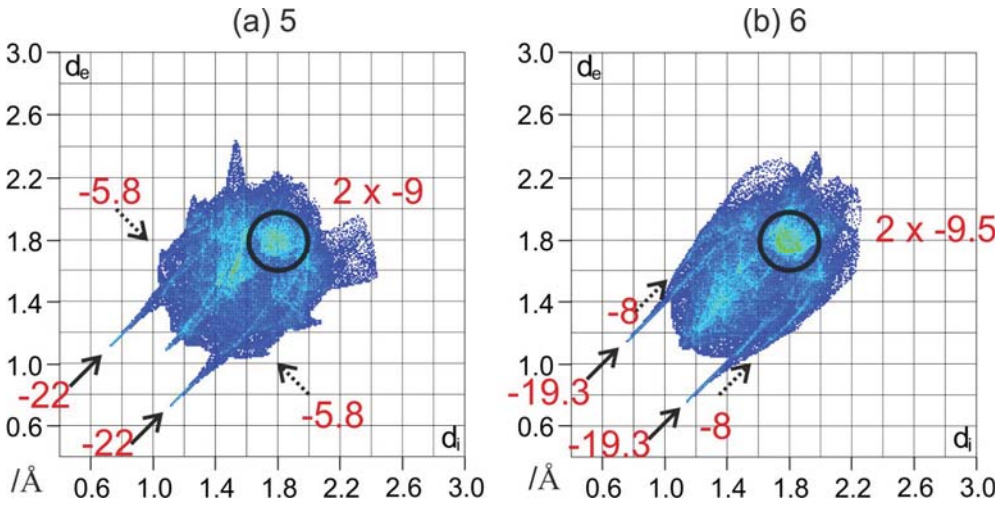

Figure S14. 2D Fingerprint plots derived from Hirshfeld surfaces[12,13] of (a) **5** and (b) **6** (Fig. 8). Red numbers correspond to PIXEL[14-16] energies of the strongest intermolecular interactions (Table S8), with N–H···N hydrogen bonds indicated with solid arrows, C–H···π or N/C–H···C short contacts with dotted arrows and the regions of π···π interactions are encircled.

2.6 Computationally Generated AH III Structure

The .res file for the calculated **AH III** is given below.

```
TITL A4_10
CELL  1.54180   31.2646   31.2646    4.4247    90.000    90.000   120.000
ZERR      18    0.0000    0.0000    0.0000     0.000     0.000     0.000
LATT   3
SYMM           - Y ,  X - Y , Z
SYMM        - X + Y ,  - X ,  Z
SFAC  C  H  N
UNIT   180  180  36
C1    1  0.14411  0.17077 -0.13796  11.00000   0.0500
C2    1  0.17663  0.15434 -0.05498  11.00000   0.0500
C3    1  0.21463  0.18079  0.15146  11.00000   0.0500
C4    1  0.21969  0.22603  0.26703  11.00000   0.0500
C5    1  0.25683  0.25672  0.47331  11.00000   0.0500
C6    1  0.25919  0.29887  0.58671  11.00000   0.0500
C7    1  0.22436  0.31218  0.49352  11.00000   0.0500
C8    1  0.18845  0.28357  0.28647  11.00000   0.0500
C9    1  0.18485  0.23981  0.16919  11.00000   0.0500
C10   1  0.10192  0.14045 -0.34787  11.00000   0.0500
H1    2  0.23603  0.12783  0.17265 11.00000 -1.20000
H2    2  0.26842  0.17970  0.41454 11.00000 -1.20000
H3    2  0.17234  0.12036 -0.15081 11.00000 -1.20000
H4    2  0.28422  0.24722  0.54804 11.00000 -1.20000
H5    2  0.28759  0.32157  0.75042 11.00000 -1.20000
H6    2  0.22598  0.34511  0.58971 11.00000 -1.20000
H7    2  0.16157  0.29356  0.20756 11.00000 -1.20000
H8    2  0.06958  0.11280 -0.22033 11.00000 -1.50000
H9    2  0.11164  0.12076 -0.51436 11.00000 -1.50000
H10   2  0.09089  0.16408 -0.46733 11.00000 -1.50000
N1    3  0.24564  0.16411  0.23342  11.00000   0.0500
N2    3  0.14760  0.21250 -0.03091  11.00000   0.0500
                                                    END
```

Reference List

1. Markvardsen, A. J.; David, W. I. F.; Johnson, J. C.; Shankland, K. *Acta Crystallogr. , Sect. A.* **2001,** *57*, 47-54.

2. David, W. I. F.; Shankland, K.; van de Streek, J.; Pidcock, E.; Motherwell, W. D. S.; Cole, J. C. *J. Appl. Crystallogr.* **2006,** *39*, 910-915.

3. Pawley, G. S. *J. Appl. Crystallogr.* **1981,** *14*, 357-361.

4. Tai, X. S.; Xu, J.; Feng, Y. M.; Liang, Z. P. *Acta Crystallogr. , Sect. E: Struct. Rep. Online* **2008,** *64*, o1026, o1026-1-o1026, o1026-6.

5. Clark, S. J.; Segall, M. D.; Pickard, C. J.; Hasnip, P. J.; Probert, M. J.; Refson, K.; Payne, M. C. *Z. Kristallogr.* **2005,** *220*, 567-570.

6. Perdew, J. P.; Burke, K.; Ernzerhof, M. *Phys. Rev. Lett.* **1996,** *77*, 3865-3868.

7. Vanderbilt, D. *Phys. Rev. B* **1990,** *41*, 7892-7895.

8. Tkatchenko, A.; Scheffler, M. *Phys. Rev. Lett.* **2009,** *102*, 073005-1-073005/4.

9. Grimme, S. *J. Comput. Chem.* **2006,** *27*, 1787-1799.

10. Spek, A. L. *Acta Crystallographica Section D* **2009,** *65*, 148-155.

11. Chisholm, J. A.; Motherwell, S. *J. Appl. Crystallogr.* **2005,** *38*, 228-231.

12. Spackman, M. A.; Jayatilaka, D. *CrystEngComm* **2009,** *11*, 19-32.

13. *CrystalExplorer,* version 3.1; Wolff, S. K.; Grimwood, D. J.; McKinnon, J. J.; Turner, M. J.; Jayatilaka, D.; Spackman, M. A. University of Western Australia: Perth: **2012**

14. Gavezzotti, A. *New J. Chem.* **2011,** *35*, 1360-1368.

15. Gavezzotti, A. *J. Phys. Chem. B* **2002,** *106*, 4145-4154.

16. Gavezzotti, A. *J. Phys. Chem. B* **2003,** *107*, 2344-2353.